

# Analysis of Extreme Light Transmission Through a Nanohole in a Metal Film Based on Discrete Sources Method

Elena Eremina<sup>1,\*</sup>, Yuri Eremin<sup>2</sup>, Natalia Grishina<sup>2</sup>, and Thomas Wriedt<sup>3</sup>

<sup>1</sup>Bremen University, Badgasteiner Str. 3, 28359 Bremen, Germany

<sup>2</sup>Moscow Lomonosov State University, Lenin's Hills, 119992 Moscow, Russia

<sup>3</sup>Institute of Materials Science, Badgasteiner Str. 3, 28359 Bremen, Germany

The effect of extreme light transmission through a nanohole in metal film deposited on a glass prism has been investigated. The Discrete Sources Method has been applied for computer simulation analysis of this effect in the evanescent wave area. It has been found that the effect appears together with Plasmon resonance of the film. The dependence of the transmitted intensity on the wavelength, incident angle, film materials and hole's filling has been analyzed.

**Keywords:** Nanohole, Discrete Sources Method, Metal Film, Evanescent Wave, Plasmon Resonance.

## 1. INTRODUCTION

The effect of Enhanced Optical Transmission (EOT) through subwavelength holes array in a metal screen detected by Ebbesen in 1988<sup>1</sup> recently found a lot of practical applications in nanooptics and biophotonics. Since the first paper on this topic published by Ebbesen et al. ten years later,<sup>2</sup> the EOT attracted considerable interest by numerous researchers. It has been found that the effect appears at certain wavelength of the incident light, which depends of the screen material. Up to now it has been detected for holes arrays and for single hole as well.<sup>1,3</sup> In a paper by Wannemacher<sup>3</sup> this effect has been explained by Surface Plasmon excitation. It is now generally agreed that Surface Plasmon Resonances (SPR) play a key role in an enhancement of light transmission through sub-wavelength apertures in noble metal screens.<sup>4,5</sup> Until now different scientific teams worldwide continue examination of transmission properties of sub-wavelength apertures in connection with development of optical antennas and biosensors.<sup>6–9</sup> Mostly those investigations correspond to the normal incidence of the light onto the screen. At the same time there are multiple practical applications, which involve evanescent wave excitation.<sup>10–12</sup> The use of evanescent waves allows avoiding some problems, for example filtering the refracted wave behind the screen from the scattered one.

In our recent paper<sup>13</sup> a new effect of extreme light transmission through a nanohole in a noble metal film deposited

on the prism surface in the area of evanescent waves has been reported. As it was found the effect appearance does not depend on the metal film thickness, hole's diameter and its filling, but it is strongly influenced by the film material. In the present paper spectral characteristics of the nanohole are modeled and analyzed. Close correlation between SPR<sup>14</sup> and Extreme Transmission Effect (ETE) has been identified.

For the modeling we used the Discrete Sources Method (DSM),<sup>15</sup> which is close to the Multiple Multipole Method.<sup>16</sup> DSM enables to consider light spectral scattering characteristics of a hole in a multilayered interface both in the propagating and evanescent wave area accounting for frequency dispersion of materials. In the following part of the paper we briefly present the basic outlines of the DSM.

## 2. SCATTERING PROBLEM STATEMENT AND DSM OUTLINES

Let the whole space be divided into three domains: air  $D_0$ , film  $D_f$  and a glass prism, which is modeled as a half-space  $D_1$ . Let the plane  $\Sigma_1$  separate a film and a glass prism and the plane  $\Sigma_f$ —air and the film. A cylindrical hole occupying a certain domain  $D_i$  with a smooth boundary  $\partial D$  is located inside the film of thickness  $d$ , bounded by the planes  $\Sigma_1$  and  $\Sigma_f$ . We assume that the symmetry axis of the hole coincides with the normal direction to  $\Sigma_1$ . Let us introduce a Cartesian coordinate system  $Oxyz$  by choosing its origin  $O$  at the prism-surface  $\Sigma_1$  in the center

\*Author to whom correspondence should be addressed.

of the hole's bottom. Let the  $Oz$  axis coincide with the symmetry axis of the hole and directed into  $D_0$ . The plane  $z = 0$  corresponds to the  $\Sigma_1$  plane (Fig. 1(a)).

We assume that the exciting field  $\{\mathbf{E}^0, \mathbf{H}^0\}$  is a linear polarized plane wave propagating from the prism domain  $D_1$  at an angle  $\theta_1$  with respect to the  $Z$ -axis. We start with the solution of the scattering problem of the plane wave  $\{\mathbf{E}^0, \mathbf{H}^0\}$  on the layered interface without the hole. The result yields field of external excitation  $\{\mathbf{E}_\zeta^0, \mathbf{H}_\zeta^0\}$ ,  $\zeta = 0, f, 1$  in domains  $D_{0,f,1}$ , which satisfy the transmission conditions at the planes  $\Sigma_{1,f}$ . While in  $D_{1,f}$  the exciting field consists of incident and reflected waves, in  $D_0$  the field includes the transmitted wave which is transformed to the evanescent one behind some critical angle. In particular, the exciting field inside the film can be represented by a linear combination of plane waves propagating up and down inside the film that is:

$$\begin{aligned} \mathbf{E}_f^0 &= w_i^{P,S} \mathbf{E}_f^{(+P,S)} + w_r^{P,S} \mathbf{E}_f^{(-P,S)}, \\ \mathbf{H}_f^0 &= w_i^{P,S} \mathbf{H}_f^{(+P,S)} + w_r^{P,S} \mathbf{H}_f^{(-P,S)} \end{aligned} \quad (1)$$

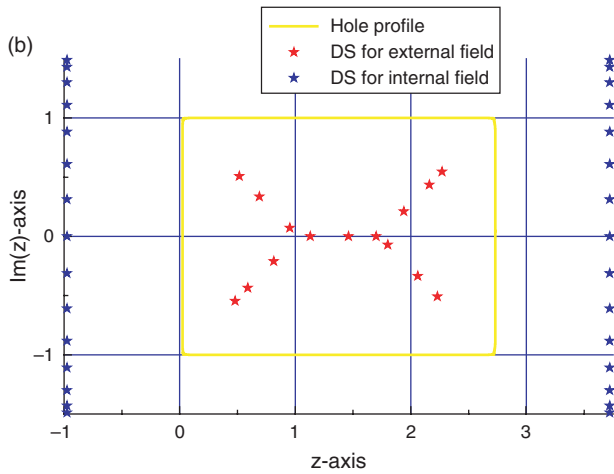
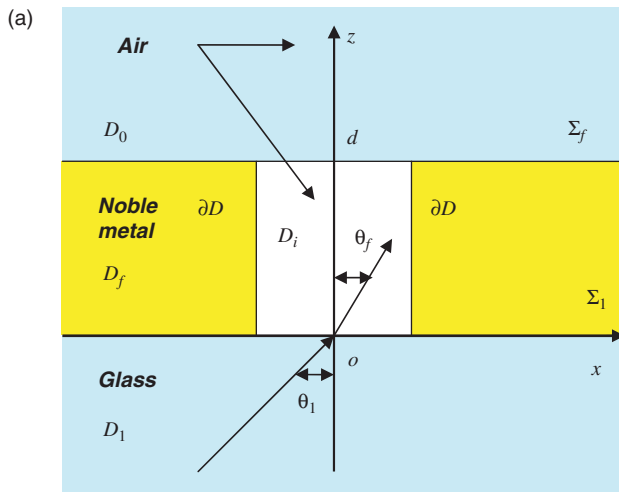


**Fig. 1.** (a) Task geometry; (b) Distribution of the Discrete Sources in the complex plane with respect to the hole profile.

where

$$\begin{aligned} \mathbf{E}_f^{(\pm)P} &= (\mp \cos \theta_f \mathbf{e}_x + \sin \theta_f \mathbf{e}_z) \chi^\pm; & \mathbf{H}_f^{(\pm)P} &= -n_f \mathbf{e}_y \chi^\pm \\ \mathbf{H}_f^{(\pm)S} &= n_f (\mp \cos \theta_f \mathbf{e}_x + \sin \theta_f \mathbf{e}_z) \chi^\pm; & \mathbf{E}_f^{(\pm)S} &= \mathbf{e}_y \chi^\pm \\ \chi^\pm &= \exp\{-jk_f(x \sin \theta_f \pm z \cos \theta_f)\}; \\ k_\zeta^2 &= k^2 \varepsilon_\zeta \mu_\zeta, & n_\zeta &= \sqrt{\varepsilon_\zeta \mu_\zeta}, \quad \zeta = 0, f, 1. \\ w_i^{P,S} &= \frac{t_{1f}^{P,S}}{1 - r_{f1}^{P,S} r_{f0}^{P,S} e_f^2}, & w_r^{P,S} &= -r_{f0}^{P,S} e_f^2 w_i^{P,S}, \\ e_f &= \exp\{-jk_f d \cos \theta_f\} \end{aligned}$$

Here  $r_{\alpha\beta}^{P,S}$ ,  $t_{\alpha\beta}^{P,S}$  are the corresponding coefficients of reflection and transmission at the interface between  $D_\alpha$  and  $D_\beta$  domains, for P- and S-polarized plane waves,<sup>17</sup>  $\varepsilon_\zeta$ ,  $\mu_\zeta$ —are the permittivity and permeability of the corresponding media,  $k = \omega/c$ ,  $\theta_f$ —transmission angle according to the Snell's law,  $\mathbf{e}_{x,y,z}$ —orthogonal basis.

Then the mathematical statement of the scattering problem for the scattering field outside  $D_i$  and the total field inside  $D_i$  can be formulated as follows:

$$\begin{aligned} \nabla \times \mathbf{H}_\zeta &= jk \varepsilon_\zeta \mathbf{E}_\zeta; & \nabla \times \mathbf{E}_\zeta &= -jk \mu_\zeta \mathbf{H}_\zeta & \text{in } D_\zeta, \\ & & & & \zeta = 0, 1, f, i \\ \mathbf{n}_p \times (\mathbf{E}_i(p) - \mathbf{E}_f(p)) &= \mathbf{n}_p \times \mathbf{E}_f^0(p), & & & p \in \partial D \\ \mathbf{n}_p \times (\mathbf{H}_i(p) - \mathbf{H}_f(p)) &= \mathbf{n}_p \times \mathbf{H}_f^0(p), & & & (2) \\ \mathbf{e}_z \times (\mathbf{E}_f(p) - \mathbf{E}_1(p)) &= 0, \\ \mathbf{e}_z \times (\mathbf{H}_f(p) - \mathbf{H}_1(p)) &= 0, & p \in \Sigma_1; \\ \mathbf{e}_z \times (\mathbf{E}_0(p) - \mathbf{E}_f(p)) &= 0, \\ \mathbf{e}_z \times (\mathbf{H}_0(p) - \mathbf{H}_f(p)) &= 0, & p \in \Sigma_f \\ \lim_{r \rightarrow \infty} \left( \sqrt{\varepsilon_\zeta} \mathbf{E}_\zeta^s \times \frac{\mathbf{r}}{r} - \sqrt{\mu_\zeta} \mathbf{H}_\zeta^s \right) &= 0, \\ & & r = |\mathbf{M}| \rightarrow \infty, & \zeta = 0, 1. \end{aligned}$$

$$(|E_f|, |H_f|) = o(\exp\{-|\text{Im}k_f|\rho\}), \quad \rho = \sqrt{x^2 + y^2} \rightarrow \infty$$

Here,  $\mathbf{e}_z$  is the unit normal vector to the planes  $\Sigma_{1,f}$ ,  $\mathbf{n}_p$  is the outward unit normal vector to  $\partial D$ ,  $k = \omega/c$ . If  $\text{Im}(\varepsilon_\zeta, \mu_\zeta) \leq 0$  (the time dependence for the fields was chosen as  $\exp\{j\omega t\}$ ) and the particle surface is smooth enough:  $\partial D \subset C^{(2,\alpha)}$ , then the above boundary-value scattering problem is uniquely solvable.<sup>18</sup>

In the frame of DSM<sup>15</sup> the approximate solution is constructed by representing the electromagnetic fields as a finite linear combination of the electric and magnetic fields of multipoles distributed over the axis of symmetry inside the scatterer or in an adjoint complex plane. Besides, the fields of multipoles analytically satisfy the transmission conditions enforced at the plane interfaces  $\Sigma_{1,f}$ . This circumstance plays a key role because of it provides an

opportunity to account for all interactions caused by fields multiple reflections between the hole and the interface analytically. Then the approximate solution satisfies Maxwell equations in the domains  $D_\zeta$ ,  $\zeta = 0, 1, f, i$ , the infinity conditions and the transmission conditions at the plane interfaces  $\Sigma_{1,f}$ . Thus, the scattering problem (2) is reduced to the problem of approximation of the exciting field  $\{\mathbf{E}_f^0, \mathbf{H}_f^0\}$  at the hole's surface  $\partial D$ . Only the amplitudes of the discrete sources (DS) are to be determined from the boundary conditions at  $\partial D$  which can be written as:

$$\begin{aligned} \mathbf{n}_p \times (\mathbf{E}_i(p) - \mathbf{E}_f(p)) &= \mathbf{n}_p \times \mathbf{E}_f^0(p), \\ \mathbf{n}_p \times (\mathbf{H}_i(p) - \mathbf{H}_f(p)) &= \mathbf{n}_p \times \mathbf{H}_f^0(p), \quad p \in \partial D \end{aligned} \quad (3)$$

To construct the fields of dipoles and multipoles that analytically satisfy the transmission conditions at the plane interfaces  $\Sigma_{1,f}$  we incorporate the Green's Tensor for a layered interface.<sup>19</sup> In the frame of DSM the approximate solution of the scattering problem is constructed additionally taking into account the rotational symmetry of the scattering problem geometry (hole together with layered interface) and the polarization of the exciting field.<sup>15</sup>

Let us consider P-polarized excitation first. To account for the axial symmetry and polarization of the exciting field we implement a plane wave resolution into a Fourier series with respect to the azimuth angle  $\varphi$ . Then for the Fourier harmonics of the external excitation the following representation holds:

$$\begin{aligned} \mathbf{E}_{f(m)}^0 &= \{\mathbf{E}_{m\rho}^{0,P}(q) \cos(m+1)\varphi; \mathbf{E}_{m\varphi}^{0,P}(q) \sin(m+1)\varphi; \\ &\quad \mathbf{E}_{mz}^{0,P}(q) \cos(m+1)\varphi\} \\ \mathbf{H}_{f(m)}^0 &= \{\mathbf{H}_{m\rho}^{0,P}(q) \sin(m+1)\varphi; \mathbf{H}_{m\varphi}^{0,P}(q) \cos(m+1)\varphi; \\ &\quad \mathbf{H}_{mz}^{0,P}(q) \sin(m+1)\varphi\} \end{aligned} \quad (4)$$

where  $q = (\rho, z)$  stands for a point located in the half plane  $\varphi = const$ . To take the polarization of the external excitation into account we should use some linear combination of electrical and magnetic multipoles deposited along the axis of symmetry.<sup>15</sup> For the scattered field representation outside the hole the following vector potentials are used

$$\begin{aligned} \mathbf{A}_{mn}^{e,f} &= \{g_m^e(q, w_n) \cos(m+1)\varphi; -g_m^e(q, w_n) \sin(m+1)\varphi; \\ &\quad -f_{m+1}(q, w_n) \cos(m+1)\varphi\}, \\ \mathbf{A}_{mn}^{h,f} &= \{g_m^h(q, w_n) \sin(m+1)\varphi; g_m^h(q, w_n) \cos(m+1)\varphi; \\ &\quad -f_{m+1}(q, w_n) \sin(m+1)\varphi\} \\ \mathbf{A}_n^{e,f} &= \{0; 0; g_0^h(q, w_n)\} \end{aligned} \quad (5)$$

Here the Fourier harmonics of the Green Tensor  $g_m^{e,h}, f_m$ , which accept the form of Weyl-Sommerfeld integrals:

$$\begin{aligned} g_m^{e,h}(q, w_n) &= \int_0^\infty J_m(\lambda\rho) v_{11}^{e,h}(z, w_n, \lambda) \lambda^{1+m} d\lambda, \\ f_m(q, w_n) &= \int_0^\infty J_m(\lambda\rho) v_{31}(z, w_n, \lambda) \lambda^{1+m} d\lambda \end{aligned} \quad (6)$$

Here  $J_m(\cdot)$  is the cylindrical Bessel function, and the multipoles are distributed along the axis of symmetry  $w_n \in Oz$  inside  $D_i$  or in an adjoined complex plane by setting  $w = z' \pm jz''$  as it was introduced in Eremin Yu. A. Presentation of Fields in Terms of Sources in the Complex Plane in the Method of Nonorthogonal Series. Sov. Phys. Dokl. 28, 6 (1983) p. 451. Typical DS distribution in the complex plane with respect to the hole profile can be observed on Figure 1(b).

The spectral functions  $v_{11}^{e,h}, v_{31}^{e,h}$  corresponding to (6) are given by

$$\begin{aligned} v_{11}^{e,h}(z, w_n, \lambda) &= \begin{cases} A_{11}^{e,h}(\lambda, w_n, d) \exp\{-\eta_0|z-d|\}, & z > d \\ \frac{\exp\{-\eta_0|z-d|\}}{\eta_f} + B_{11}^{e,h} \exp\{-\eta_f|z-d|\} \\ + C_{11}^{e,h} \exp\{-\eta_f z\}, & d > z > 0 \\ D_{11}^{e,h}(\lambda, w_n, d) \exp\{-\eta_1 z\}, & z < 0 \end{cases} \\ v_{31}^{e,h}(z, w_n, \lambda) &= \begin{cases} A_{31}^{e,h}(\lambda, w_n, d) \exp\{-\eta_0|z-d|\}, & z > d \\ B_{31}^{e,h} \exp\{-\eta_f|z-d|\} + C_{31}^{e,h} \exp\{-\eta_f z\}, \\ & d > z > 0 \\ D_{31}^{e,h}(\lambda, w_n, d) \exp\{\eta_1 z\}, & z < 0 \end{cases} \end{aligned}$$

Here  $\eta_\zeta^2 = \lambda^2 - k_\zeta^2$ ,  $k_\zeta^2 = k^2 \varepsilon_\zeta \mu_\zeta$ ,  $\zeta = 0, f$ .

The associated spectral coefficients  $A_{\alpha\beta}^{e,h}, B_{\alpha\beta}^{e,h}, C_{\alpha\beta}^{e,h}, D_{\alpha\beta}^{e,h}$  are determined from the following one-dimensional transmission conditions imposed at  $z = 0, d$ :

$$\begin{aligned} [v_{11}^e] &= \left[ \frac{1}{\mu} \frac{\partial v_{11}^e}{\partial z} \right] = 0, \quad [v_{11}^h] = \left[ \frac{1}{\varepsilon} \frac{\partial v_{11}^h}{\partial z} \right] = 0, \\ \left[ \frac{1}{\mu} v_{31}^e \right] &= 0, \quad \left[ \frac{1}{\varepsilon \mu} \frac{\partial v_{31}^e}{\partial z} \right] = - \left[ \frac{1}{\varepsilon \mu} \right] v_{11}^e, \\ \left[ \frac{1}{\varepsilon} v_{31}^h \right] &= 0, \quad \left[ \frac{1}{\varepsilon \mu} \frac{\partial v_{31}^h}{\partial z} \right] = - \left[ \frac{1}{\varepsilon \mu} \right] v_{11}^h \end{aligned}$$

Here square brackets  $[.]$  stay for the jump of values across the interface. In particular, the equality  $v_{31}^e = v_{31}^h$  holds at  $d > z > 0$ . For the P-polarized total field representation inside the hole the following vector potentials are used<sup>15</sup>

$$\begin{aligned} \mathbf{A}_{mn}^{e,i} &= \{Y_m(q, w_n^i) \cos(m+1)\varphi; \\ &\quad -Y_m(q, w_n^i) \sin(m+1)\varphi; 0\} \\ \mathbf{A}_{mn}^{h,i} &= \{Y_m(q, w_n^i) \sin(m+1)\varphi; \\ &\quad Y_m(q, w_n^i) \cos(m+1)\varphi; 0\}; \\ \mathbf{A}_n^{e,i} &= \{0; 0; Y_0(q, w_n^i)\} \end{aligned} \quad (7)$$

Here  $Y_m(q, w_n^i) = h_m^{(2)}(k_i R_{qw_n^i}) \cdot (k_i \rho / R_{qw_n^i})^m$ ,  $R_{qw_n^i} = \sqrt{\rho^2 + (z - w_n^i)^2}$  and  $h_m^{(2)}(\cdot)$  are spherical Hankel functions. Let us emphasize that the sets  $\{w_n^i\}$  and  $\{w_n\}$  are different and that  $w_n^i$  are located outside  $D_i$ .

Thus for the scattered fields in  $D_{0,f,1}$  which satisfy the transmission conditions at  $\Sigma_{1,f}$  and total field inside  $D_i$  the following representation is valid:

$$\begin{aligned} \mathbf{E}_{\zeta,N} &= \sum_{m=0}^M \sum_{n=1}^{N_m^\xi} \left\{ p_{mn}^\xi \frac{j}{k \varepsilon_\zeta \mu_\zeta} \nabla \times \nabla \times \mathbf{A}_{mn}^{e,\zeta} + q_{mn}^\xi \frac{1}{\varepsilon_\zeta} \nabla \times \mathbf{A}_{mn}^{h,\zeta} \right\} \\ &+ \sum_{n=1}^{N_0^\xi} r_n^\xi \frac{j}{k \varepsilon_\zeta \mu_\zeta} \nabla \times \nabla \times \mathbf{A}_n^{e,\zeta}; \quad (8) \\ \mathbf{H}_{\zeta,N} &= \frac{j}{k \mu_\zeta} \nabla \times \mathbf{E}_{\zeta,N}(M), \quad \zeta = 0, f, 1, i; \quad \xi = f, i \end{aligned}$$

The approximate solution for the S-polarized excitation can be constructed in a similar way. Accounting that the Fourier harmonics for the exciting plane wave can be written as

$$\begin{aligned} \mathbf{E}_{f(m)}^0 &= \{\mathbf{E}_{m\rho}^{0,S}(q) \sin(m+1)\varphi; \mathbf{E}_{m\varphi}^{0,S}(q) \cos(m+1)\varphi; \\ &\quad \mathbf{E}_{mz}^{0,S}(q) \sin(m+1)\varphi\} \quad (9) \\ \mathbf{H}_{f(m)}^0 &= \{\mathbf{H}_{m\rho}^{0,S}(q) \cos(m+1)\varphi; \mathbf{H}_{m\varphi}^{0,S}(q) \sin(m+1)\varphi; \\ &\quad \mathbf{H}_{mz}^{0,S}(q) \cos(m+1)\varphi\} \end{aligned}$$

Here the following electric and magnetic vector potentials corresponding to the multipoles are employed:

$$\begin{aligned} \mathbf{A}_{mn}^{e,f} &= \{g_m^e(q, w_n) \sin(m+1)\varphi; g_m^e(q, w_n) \cos(m+1)\varphi; \\ &\quad -f_{m+1}(q, w_n) \sin(m+1)\varphi\}, \\ \mathbf{A}_{mn}^{h,f} &= \{g_m^h(q, w_n) \cos(m+1)\varphi; -g_m^h(q, w_n) \sin(m+1)\varphi; \\ &\quad -f_{m+1}(q, w_n) \cos(m+1)\varphi\}, \\ \mathbf{A}_n^{h,f} &= \{0; 0; g_0^e(q, w_n)\} \quad (10) \end{aligned}$$

The vector potential for the total field inside  $D_i$  accept the following form

$$\begin{aligned} \mathbf{A}_{mn}^{e,i} &= \{Y_m(q, w_n^i) \sin(m+1)\varphi; \\ &\quad -Y_m(q, w_n^i) \cos(m+1)\varphi; 0\} \\ \mathbf{A}_{mn}^{h,i} &= \{Y_m(q, w_n^i) \cos(m+1)\varphi; \\ &\quad Y_m(q, w_n^i) \sin(m+1)\varphi; 0\}; \quad (11) \\ \mathbf{A}_n^{h,i} &= \{0; 0; Y_0(q, w_n^i)\} \end{aligned}$$

Then for the scattered fields in  $D_{0,1,f}$ , which satisfy the transmission conditions at  $\Sigma_{1,f}$  and the total field inside  $D_i$  the following representation is valid:

$$\begin{aligned} \mathbf{E}_{\zeta,N} &= \sum_{m=0}^M \sum_{n=1}^{N_m^\xi} \left\{ p_{mn}^\xi \frac{j}{k \varepsilon_\zeta \mu_\zeta} \nabla \times \nabla \times \mathbf{A}_{mn}^{e,\zeta} + q_{mn}^\xi \frac{1}{\varepsilon_\zeta} \nabla \times \mathbf{A}_{mn}^{h,\zeta} \right\} \\ &+ \sum_{n=1}^{N_0^\xi} r_n^\xi \frac{j}{k \varepsilon_\zeta \mu_\zeta} \nabla \times \nabla \times \mathbf{A}_n^{h,\zeta}; \quad (12) \\ \mathbf{H}_{\zeta,N} &= \frac{j}{k \mu_\zeta} \nabla \times \mathbf{E}_{\zeta,N}(M), \quad \zeta = 0, f, 1, i; \quad \xi = f, i \end{aligned}$$

The completeness of the system of dipoles and multipoles guarantees the convergence of the approximate solution (8), (12) to the exact one.<sup>20</sup>

### 3. NUMERICAL SCHEME OF THE DSM

In this section a short description of the numerical scheme of DSM is presented. As mentioned above, the representations (8) and (12) satisfy all the conditions of the scattering problem (2) except the transmission conditions at the hole's surface (3). These conditions are used to determine the unknown amplitudes of the DS  $\{p_{mn}^\xi, q_{mn}^\xi, r_n^\xi\}$ . Note that we need to compute the coefficients  $\{p_{mn}^f, q_{mn}^f, r_n^f\}_{n=1}^{N_m^f}$  and  $\{p_{mn}^i, q_{mn}^i, r_n^i\}_{n=1}^{N_m^i}$  only. Because of by using Green's Tensor we constructed unitary representation of the field outside  $D_i$  with the same amplitudes. Let us remind that the scattering problem geometry is axially symmetric with respect to the  $Z$ -axis and the DS can be distributed over the axis of symmetry. To account for the singularities of the scattered field continuation inside the hole we construct an analytic continuation of the DS's positions to the adjoined complex plane  $\{w_n\}_{n=1}^{N_m^f}$ .<sup>20</sup> Besides, the DS for the internal field representation  $\{w_n^i\}_{n=1}^{N_m^i}$  are placed in the complex plane in such a way that their projections to the real axis ( $Oz$ ) do not touch the domain  $D_i$  (see Fig. 1(b)). Therefore, fulfilling the transmission conditions (3) at the surface  $\partial D$  can be reduced to a sequential set of 1D transmission problems for the Fourier harmonics of the fields (see (4), (5), (7) for P-polarization or (9)–(11) for S-polarization). Thus, instead of matching the fields on the scattering surface (see (3)), we match their Fourier harmonics separately by reducing the approximation problem on the surface  $\partial D$  to a set of 1D problems enforced at the particle surface generatrix  $\mathfrak{S}$ . By solving these problems one can determine the DS amplitudes.

There are various numerical schemes for the evaluation of the amplitudes. It has been found that most stable results can be obtained by combining the Generalized Point-Matching Technique and a Pseudo-Solution of corresponding over-determined systems of linear equations.<sup>15</sup> As a rule we choose the number of DS ( $N_m^f + N_m^i$ ) depending on the number of Fourier harmonics  $m$  twice less than the number of the matching point distributed over  $\mathfrak{S}$ . Then we make a separation between the DS numbers for the scattered field  $N_m^f$  and the internal one  $N_m^i$  following the film-hole refractive index values. The higher refractive index is the more DS are required.

For DSM is a direct method, it does not require an iterative solver. Therefore, it allows solving the scattering problem for the complete set of incident angles  $\theta_1$  and both polarizations (P and S) at once.<sup>15</sup> This is advantageous especially for investigation of nano-size scatterers compared to methods similar to Discrete Dipole Approximation (DDA), Volume Integral Equation (VIE) or Finite Difference Time Domain (FDTD), which require

application of an iterative scheme. Besides, the DSM numerical scheme provides an opportunity to control the actual convergence of the approximate solution to the exact one by posterior error estimation.<sup>16</sup>

After the amplitudes of the DS have been determined, one can calculate the far field pattern  $\mathbf{E}_\infty(\theta, \varphi)$  of the scattered field, which is determined at the upper semi-sphere  $\Omega = \{0^\circ \leq \theta \leq 90^\circ, 0^\circ \leq \varphi \leq 360^\circ\}$  and is given by

$$\mathbf{E}_0(M)/|\mathbf{E}^0(z=0)| = \frac{\exp\{-jk_0r\}}{r} \mathbf{E}_\infty(\theta, \varphi) + o(r^{-1}),$$

$$z > d, r = |M| \rightarrow \infty$$

We asymptotically estimate the Weyl-Sommerfeld integrals involved in (6),<sup>19</sup> which yields the following representation for the  $\theta, \varphi$ -components of the far field pattern corresponding to the representation (8):

$$E_{\infty,\theta}^P(\theta, \varphi) = \frac{jk_0}{\varepsilon_0} \sum_{m=0}^M (jk_0 \sin \theta)^m \cos(m+1)\varphi$$

$$\times \sum_{n=1}^{N_m^f} \{P_{nm}^f [\bar{g}_{nm}^e \cos \theta + jk_0 \sin^2 \theta \bar{f}_{nm}^-] + q_{nm}^f \bar{g}_{nm}^h\} - \frac{jk_0}{\varepsilon_0} \sin \theta \sum_{n=1}^{N_0^f} r_n^f \bar{g}_{n0}^h, \quad (13)$$

$$E_{\infty,\varphi}^P(\theta, \varphi) = -\frac{jk_0}{\varepsilon_0} \sum_{m=0}^M (jk_0 \sin \theta)^m \sin(m+1)\varphi$$

$$\times \sum_{n=1}^{N_m^f} \{P_{nm}^f \bar{g}_{nm}^e + q_{nm}^f [\bar{g}_{nm}^h \cos \theta + jk_0 \sin^2 \theta \bar{f}_{nm}^-]\}$$

For S-polarized excitation following to representation (12) one gets

$$E_{\infty,\theta}^S(\theta, \varphi) = \frac{jk_0}{\varepsilon_0} \sum_{m=0}^M (jk_0 \cos \theta)^m \cos(m+1)\varphi$$

$$\times \sum_{n=1}^{N_m^f} \{P_{nm}^f [\bar{g}_{nm}^e \cos \theta + jk_0 \sin^2 \theta \bar{f}_{nm}^-] - q_{nm}^f \bar{g}_{nm}^h\},$$

$$E_{\infty,\varphi}^S(\theta, \varphi) = \frac{jk_0}{\varepsilon_0} \sum_{m=0}^M (jk_0 \cos \theta)^m \sin(m+1)\varphi$$

$$\times \sum_{n=1}^{N_m^f} \{P_{nm}^f \bar{g}_{nm}^e - q_{nm}^f [\bar{g}_{nm}^h \cos \theta + jk_0 \sin^2 \theta \bar{f}_{nm}^-]\}$$

$$+ \frac{jk_0}{\varepsilon_0} \sin \theta \sum_{n=1}^{N_0^f} r_n^f \bar{g}_{n0}^e \quad (14)$$

Where the corresponding spectral functions  $\bar{g}_{nm}^{e,h}, \bar{f}_{nm}$  accept the form:

$$\bar{g}_{nm}^{e,h}(\theta) = jk_0 \cos \theta \exp\{jk_0 d \cos \theta\} A_{11}^{e,h}(k_0 \sin \theta, z_n, d),$$

$$\bar{f}_{nm}(\theta) = jk_0 \cos \theta \exp\{jk_0 d \cos \theta\} A_{31}^e(k_0 \sin \theta, z_n, d)$$

Hence, after the unknown amplitudes of DS are determined, the far field patterns for P/S polarization (13), (14) are represented as finite linear combinations of elementary functions. This circumstance ensures a low costs computer analysis of the scattering characteristics in the far zone.

#### 4. NUMERICAL RESULTS AND DISCUSSION

We are mostly interested in scattered intensity in  $D_0$  which is calculated as:

$$I^{P,S}(\theta_1, \theta, \varphi) = |E_{\infty,\theta}^{P,S}(\theta_1, \theta, \varphi)|^2 + |E_{\infty,\varphi}^{P,S}(\theta_1, \theta, \varphi)|^2 \quad (15)$$

where  $E_{\infty,\theta,\varphi}^{P,S}(\theta_1, \theta, \varphi)$  are the components of the far field pattern for a P and S polarized incident wave, in a spherical coordinate system  $\theta, \varphi$  (see 13–14).

We consider the Scattering Cross-Section (SCS), which represents the total integrated intensity scattered (transmitted) into the upper semi-sphere  $\Omega = \{0^\circ \leq \theta \leq 90^\circ, 0^\circ \leq \varphi \leq 360^\circ\}$ :

$$\sigma^{P,S}(\theta_1) = \int_{\Omega} I^{P,S}(\theta_1, \theta, \varphi) d\omega \quad (16)$$

Let  $\theta_0$  be a transmission angle of the plane wave in  $D_0$ . Snell's law in this case yields:  $\sin \theta_0 = (n_1/n_0) \sin \theta_1$ . As  $|n_1| > |n_0|$  with increase of incident angle  $\theta_1$  from 0 till  $\pi/2$  one can get  $|\sin \theta_0| > 1$ . This circumstance requires using of a corresponding branch for  $\cos \theta_0 = -j\sqrt{\sin^2 \theta_0 - 1}$  which assures an outgoing wave. Hence, beyond the critical angle  $\theta_c = \arcsin n_0/n_1$  in the upper half-space an evanescent wave appears, which propagates along the interface and damps in the normal ( $z > d$ ) direction to the interface  $\Sigma_f$ :

$$\chi^+ = \exp\{-jk_0 x \sin \theta_0\} \exp\{-k_0 z \sqrt{\sin^2 \theta_0 - 1}\}$$

Next, we will present some numerical results obtained by using the DSM model and discuss them shortly. In our recent paper<sup>13</sup> the dependence of the transmitted intensity on the incident angle has been investigated. In this paper we consider the spectral characteristics of the transmitted light as well. We examine the scattering properties of the hole excited by a linear polarized plane wave with an exciting wavelength within the range of  $\lambda = 400\text{--}700$  nm. In the present paper we consider the cylindrical hole of diameter  $D = 40$  nm in a metal film of thickness  $d = 55$  nm deposited on glass prism. As film materials mostly silver (Ag) and gold (Au) are used, but some selective results for other metals are presented as well. For the prism material we take BK7 glass. The refractive indices of the film material and the glass depending from the wavelength are taken from the paper of Lynch and Hunter.<sup>21</sup>

In Figure 2 the numerical results for SCS (16) versus wavelength for different incident angles  $\theta_1 = 0^\circ, 42^\circ, 44^\circ$  are presented. From the figure one can see, that while the

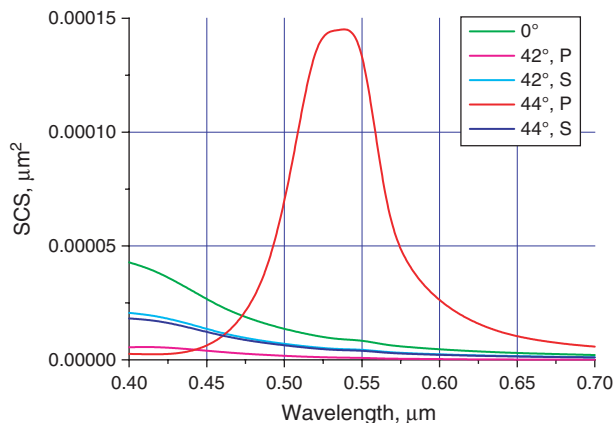


**Fig. 2.** SCS versus wavelength for the cylindrical hole  $D = 40$  nm, in Ag film  $d = 55$  nm, on a glass prism. Different incident angles.

curves for S-polarized external excitation monotonically decrease, the curve for P-polarized light for incidence  $\theta_1 = 44^\circ$  has a maximum at about  $\lambda = 532$  nm ( $\text{Re}\epsilon_f \cong -10.2$ ). The incident angle  $\theta_1 = 44^\circ$  is located beyond the critical angle (which is equal to  $\theta_c = 41.2^\circ$  for the system glass-air) in the area where evanescent wave appears in  $D_0$ . In Figure 3 similar results are presented for the hole in Au film. A closer look shows that the behaviour of the SCS curves is similar to the case of Ag film, but the P-polarized curve reaches its maximum in the vicinity of  $\lambda = 670$  nm ( $\text{Re}\epsilon_f \cong -11.5$ ).

In Figure 4 the SCS curves versus incident angle for the same hole in Ag and Au films are presented for the fixed wavelength  $\lambda = 532$  nm. While the curves for S-polarized light demonstrate just a slight decay, the P-polarisation curves both for Ag and Au film drop down behind the critical angle and then sharply jump up by two orders at the incidence near  $44^\circ$ . At the same time the maximum value of SCS for Ag film seems to be more pronounced.

For this particular case we would like to describe the DSM application in details. In the application two

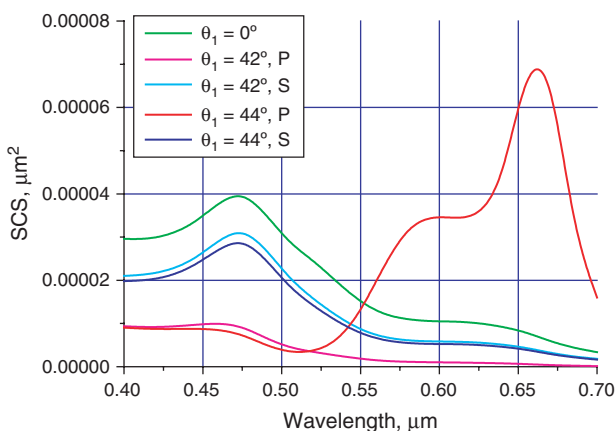


**Fig. 3.** SCS for the hole in Au film on a glass prism, different incident angles.

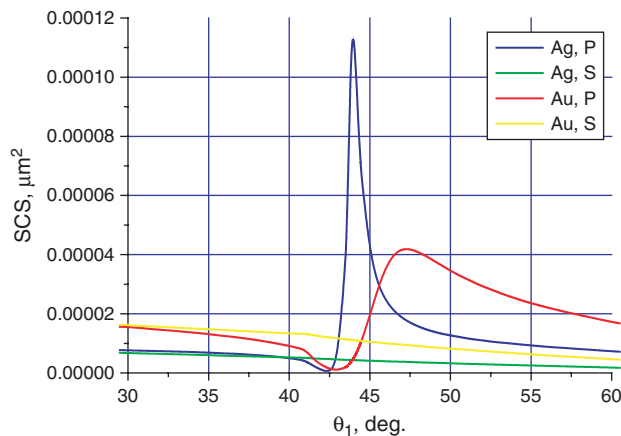


**Fig. 4.** SCS versus incident angle for the hole in Ag and Au films on glass prism,  $\lambda = 532$  nm.

( $M = 0, 1$ ) Fourier harmonics plus 2 independent on  $\varphi$  harmonics (P and S) are considered. The corresponding DS numbers for the scattered field representation are  $N_0^f = 30$ ,  $N_1^f = 24$ . The same numbers were chosen for the internal field representation. Associated distribution of the DS in the complex plane is shown in Figure 1(b). The corresponding matrix dimension for  $M = 0$  is  $216 \times 120$ , for  $M = 1 - 216 \times 96$ , for  $\varphi$  independent harmonics  $-108 \times 60$ . On a laptop Centrino Duo 2 GHz with 2 Gb RAM the calculation for 119 incident angles took 3 m 24 s. Estimated result error was about 1.4%. The most time consuming procedure seems to be the Weyl-Sommerfeld integrals estimation with a guarantee error less than  $10^{-8}$ .

In Figure 5 similar results are presented for the hole  $D = 40$  nm in Ag and Au films, but for the wavelength  $\lambda = 670$  nm associated with the maximum value of SCS for the Au film. Here we observe a similar behaviour: both Ag and Au P-polarized curves demonstrate first slight minima and then sharp maxima, but in this case the maximum SCS value for Au is much higher. From the observations we

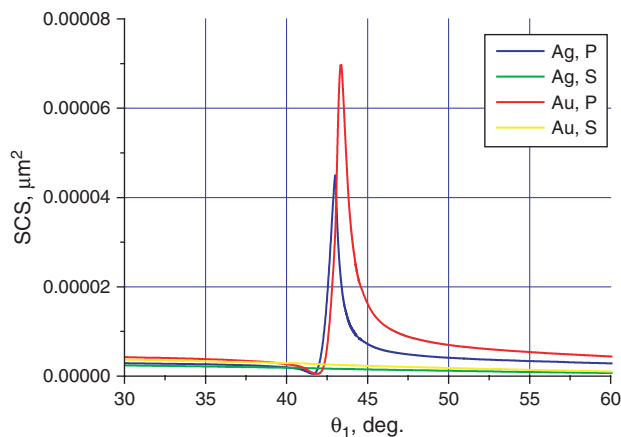


**Fig. 5.** SCS versus incident angle for the hole in Ag and Au films on glass prism,  $\lambda = 670$  nm.

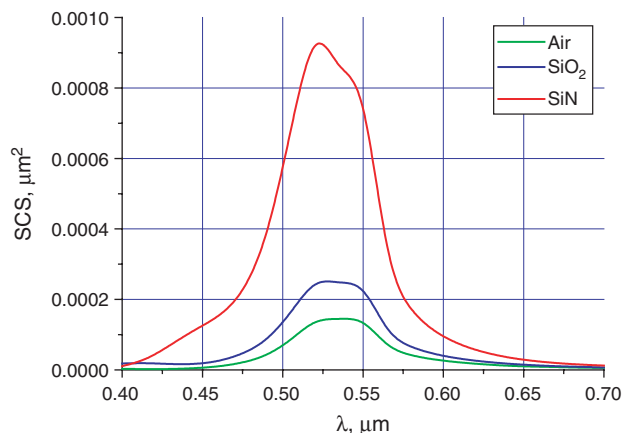


**Fig. 6.** SCS for the hole in Ag film,  $\theta_1 = 44^\circ$ . P-polarization, different fillings inside the hole.

can conclude that while both P-polarized curves for Ag and Au films demonstrate SCS maxima at the incidence nearby  $44\text{--}45^\circ$ , the maximum seems to be more observable at the wavelengths corresponding to the maxima for the spectral curves.

For the next 2 figures we will restrict our consideration just to P-polarized light, as S-polarization does not seem to be of interest for our demonstrations. In Figure 6 numerical results for the same hole filled with different materials: air,  $\text{SiO}_2$  and SiN in Ag film for  $\theta_1 = 44^\circ$  are shown. From the presented SCS results one can see that the maximum accepts higher amplitude with an increase of the filling refractive index. Let us now have a closer look at the influence of the film materials on the spectral behaviour of SCS. In Figure 7 the SCS versus wavelength for P-polarized excitation for the same hole, but different film materials are presented. As film materials besides Ag and Au, also copper (Cu) and platinum (Pt) have been considered. From the Figure 7 one can see that while Au, Ag and Cu demonstrate at least one maximum in presented wavelength range, Pt shows a simple monotonic behaviour.

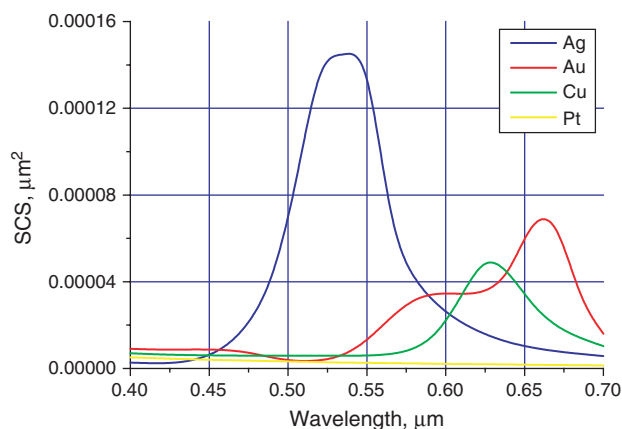


**Fig. 7.** SCS for the hole in film,  $\theta_1 = 44^\circ$ ,  $\lambda = 532$  nm. P-polarization, different film materials.

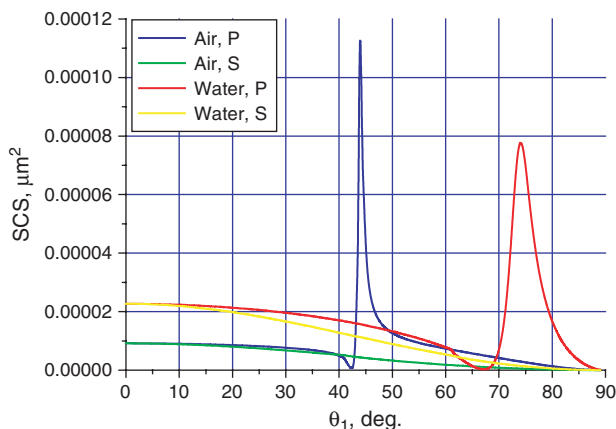


**Fig. 8.** SCS for the hole in Ag film,  $\lambda = 532$  nm. Different fillings of the upper half-space.

For the Cu film the maximum value is achieved at ( $\text{Re}\epsilon_f \cong -11.5$ ). Between the other materials, Ag exhibits the highest maximum amplitude.

We now would like to analyse the influence of critical angle value on the ETE. The evanescent waves appear in the area of lower refractive index when the incident angle exceeds the critical one  $\theta_c = \arcsin(n_0/n_1)$ . To check the influence of the value of critical angle we now consider the case when the upper half space is filled with water. In Figure 8 the comparison of SCS for the same hole in Ag film is depicted for cases when the upper half-space is filled with air ( $\theta_c \cong 41.2^\circ$ ) and water ( $\theta_c \cong 61.1^\circ$ ). The comparison indicates that in case of water the position of the maximum shifts to the higher incident angle, which corresponds to the area of evanescent waves for the system glass-water.

Let us assume that the prism  $D_1$  is made from different materials. As materials we take besides BK7 glass with  $n_1 = 1.52$  ( $\theta_c \cong 41.2^\circ$ ), SiN with  $n_1 = 2.034$  ( $\theta_c \cong 29.4^\circ$ ), and air with  $n_1 = 1.0$  as well. In cases of glass and SiN beyond the critical angles we have the area of

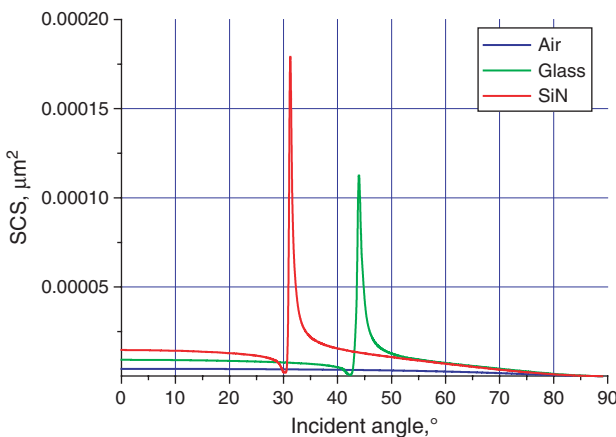


**Fig. 9.** SCS for the hole in Ag film for P-polarization,  $\lambda = 670$  nm. Different prism materials.

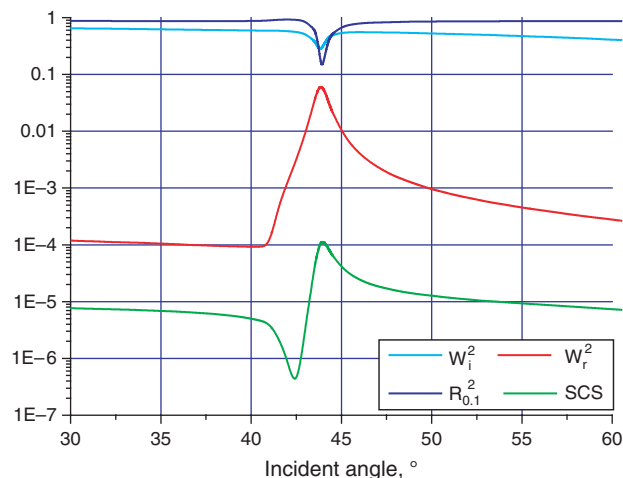


Fig. 10. SCS for the hole in Ag film, P-polarization,  $\lambda = 532$  nm.

evanescent wave, in case of air in  $D_1$  no evanescent wave appears, because of  $D_1$  and  $D_0$  have the same refractive index. Corresponding results are presented in Figure 9. From the results one can see that in case of air, when there is no evanescent wave, the curve has a strongly monotonic behaviour. In cases of glass and SiN there are sharp maxima in the area of evanescent wave.

From the results presented above, we can conclude that while the values of the SCS peaks may be manipulated by varying the film material, hole filling or the wavelength, the position of the ETE peaks with respect to the incident angle stays the same. This occurs because of varying the film material does not affect the critical angle value, which depends on refractive indices of  $D_1$  and  $D_0$  only.

To clarify the nature of the ETE we now would like to analyze the behaviour of the fields inside a film versus incident angle. In Figures 10 and 11 the SCS is shown together with the amplitudes  $|w_i^p|^2$  of the plane wave propagating from the interface  $\Sigma_1$  up and  $|w_r^p|^2$  of the plane wave propagating from the interface  $\Sigma_f$  down introduced in (1) (see Fig. 12). Besides, we consider the coefficient

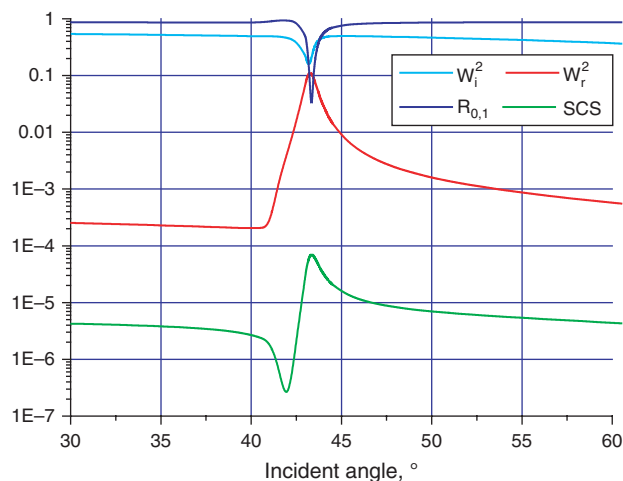


Fig. 11. SCS for the hole in Au film, P-polarization,  $\lambda = 670$  nm.

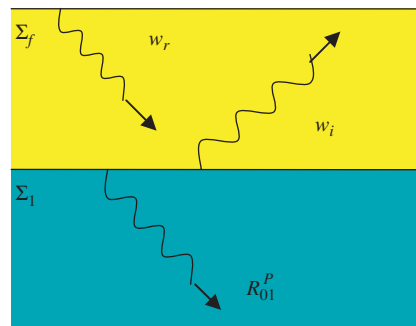


Fig. 12. Plane waves inside a film and the corresponding reflection coefficients.

of the total reflection the exciting P-polarized plane wave from the layered structure prism-film-air:

$$R_{01}^p(\theta_1) = \frac{r_{1f}^p + r_{f0}^p \exp\{-2ik_f \cos \theta_f d\}}{1 + r_{1f}^p r_{f0}^p \exp\{-2ik_f \cos \theta_f d\}}$$

From the results presented in Figures 10 and 11 we can observe that the curves for  $|R_{01}^p|^2$  and  $|w_i^p|^2$  demonstrate minima at an incidence nearby  $44^\circ$ . At the same time the curve for  $|w_r^p|^2$  demonstrates strong correlation with SCS curve. They indicate an increase of values beyond the critical angle and reach their maxima at the same angle of about  $44^\circ$ . Thus, the ETE we observe is caused by two circumstances:

- (a) SPR appearance when  $|R_{01}^p|^2$  reaches its minimum value and therefore more energy penetrates into the film;
- (b) increase of the amplitude of  $|w_r^p|^2$  from the upper interface  $\Sigma_f$  yields stronger excitation of the film's inhomogeneity (hole) especially in the evanescent wave area when the wave can not penetrate into  $D_0$ .

To summarise our discussion, we can conclude that the excitation of the evanescent waves plays the key role in the ETE appearance. An enhancement of the fields inside the noble metal film and the energy distribution between two plane waves seems to be important for the ETE. The effect arising does not depend on the film thickness, hole's diameter and filling.<sup>9</sup> In this paper we have demonstrated that it strongly depends on the film material. It was shown that the ETE seems to be more observable at those wavelengths where the corresponding spectral maximum of SCS is achieved and these wavelengths depend on the film material only.

### 5. CONCLUSION

In the present paper the spectral characteristics of light scattering by a nanohole in a metal film on a glass prism have been analyzed. It has been shown that the Extreme Transmission Effect seems to be more observable at those wavelengths where the corresponding spectral maximum of the Scattering Cross-Section is achieved. Moreover it was found, that this maximum is reached, when the real

part of the film permittivity depending of the wavelength belongs to a very narrow range of values  $[-11.5, -10.2]$ . This seems to be a necessary condition for the maximum appearance. Hence, the effect strongly depends on the film material, which for practical applications can be chosen a priori following the condition above. Close correlation between Surface Plasmon Resonance and Extreme Transmission Effect has been determined. It has been shown that the excitation of the evanescent waves plays the key role in the Extreme Transmission Effect due to an increase of the amplitude of the plane wave reflected from the upper interface, which yields stronger excitation of the hole. This fact leads to an increase of the scattered field intensity. Let us emphasize that the extreme transmission occurs as well for other types of film inhomogeneties: particles, inclusions, etc.

**Acknowledgment:** We gratefully acknowledge funding of this research by Deutsche Forschungsgemeinschaft (DFG) and the Russian Foundation for Basic Research (RFBR).

## References

1. T. Thio, *Am. Scientist* 94, 40 (2006).
2. T. W. Ebbesen, H. J. Lezec, H. F. Ghaemi, T. Thio, and P. A. Wolff, *Nature* 391, 667 (1998).
3. R. Wannemacher, *Opt. Comm.* 195, 107 (2001).
4. C. Genet and T. W. Ebbesen, *Nature* 225, 39 (2007).
5. F. J. G. de Abajo, *Reviews of Modern physics* 79, 1267 (2007).
6. C. Sönnichsen, A. C. Duch, G. Steininger, M. Koch, G. von Plessen, and J. Feldmann, *Appl. Phys. Lett.* 76, 140 (2000).
7. K. L. Shuford, S. K. Gray, M. A. Ratner, and G. C. Schatz, *Chem. Phys. Lett.* 435, 123 (2007).
8. G. S. Eom, D. Yang, S. Lee, S. Park, Y. Lee, and J. W. Hahn, *J. Appl. Phys.* 101, 103101-1 (2007).
9. L. Yin, V. K. Vasko-Vlasov, A. Rydh, J. Pearson, U. Welp, S.-H. Chang, S. K. Gray, G. C. Schatz, D. B. Brown, and C. W. Kimball, *Appl. Phys. Lett.* 85, 467 (2004).
10. L. Helden, E. Eremina, Y. Eremin, N. Riefler, C. Hertlein, C. Bechinger, and T. Wriedt, *Appl. Optics* 45, 7299 (2006).
11. M. J. Jory, P. S. Cann, and J. R. Sambles, *Appl. Phys. Lett.* 83, 3006 (2003).
12. J. A. Porto, P. Johansson, S. P. Apell, and T. Lopez-Rios, *Phys. Rev. B* 67, 085409-1 (2003).
13. E. Eremina, Y. Eremin, N. Grishina, and T. Wriedt, *Opt. Comm.* 281, 3581 (2008).
14. A. V. Zayats, I. I. Smolyaninov, and A. A. Maradudin, *Phys. Reports* 408, 131 (2005).
15. Yu. A. Eremin, *J. Comm. Technology and Electronics* 45, 269 (2000).
16. Ch. Hafner, The Multiple Multipole Program (MMP) and the Generalized Multipole Technique (GMT), edited by Th. Wriedt, Generalized Multipole Techniques for Electromagnetic and Light Scattering, Elsevier, Amsterdam (1999).
17. W. C. Chew, *Waves and Fields in Inhomogeneous Media*, IEEE Press, NY (1995).
18. D. Colton and R. Kress, *Inverse Acoustic and Electromagnetic Scattering Theory*, Springer, Berlin (1992).
19. Y. Eremin, N. Orlov, and A. Sveshnikov, Generalizes Multipole Techniques for Electromagnetic and Light Scattering, edited by T. Wriedt, Elsevier Science, Amsterdam (1999), p. 39.
20. A. Doicu, Yu. Eremin, and T. Wriedt, *Acoustic and Electromagnetic Scattering Analysis using Discrete Sources*, Academic Press, London (2000).
21. D. W. Lynch and W. R. Hunter, *Handbook of Optical Constants of Solids 1*, edited by E. D. Palik, Academic Press, San Diego (1985).

Received: 25 September 2008. Accepted: 28 October 2008.